

Analytical Calculation on the Load-Displacement Curve of Grouted Soil Anchors

Zejun Yang^{1,2}, Jiangong Chen^{1,2,*}, Haiquan Zhang^{1,2}, Xinyao Zhao^{1,2} and Hao Li³

¹College of Civil Engineering, Chongqing University, Chongqing 400045, China

²Key Laboratory of New Technology for Construction of Cities in Mountain Area (Chongqing University), Ministry of Education, Chongqing 400045, China

³School of Civil Engineering, University of Leeds, Leeds, LS2 9JT, United Kingdom

Received 7 January 2018; Accepted 2 May 2018

Abstract

The load-displacement curve of anchors can be used as a basis for quality tests, and it is also important in the stability analysis of the combined supporting structure of anchors. Most of the existing analytical methods can only solve the partial pullout process of grouted soil anchors and obtain local load-displacement curves. To obtain a complete load-displacement curve, mechanical differential equations for the anchoring section in each stage were derived in this study based on a softening shear model of the anchor-soil interface and a load transfer model of the anchoring section. Combined with boundary conditions, the displacement, axial force, and shear stress distributions along the anchoring section and the analytical solutions for the load-displacement curve in the entire pullout process of anchors were obtained. The accuracy of the proposed method was verified by a pullout test on a foundation pit in Chongqing, China. Results show that a complete load-displacement curve is obtained with the proposed analytical method and a theoretical curve is consistent with a field pullout curve. The shear stress on the anchoring section is irregularly and non-uniformly distributed with a single peak. The load-displacement curve is influenced by the changes in parameters, such as anchorage length, anchorage radius, elastic modulus of the anchoring section, and residual shear coefficient. The present study accurately simulates the entire pullout process of anchors, determines their ultimate bearing capacity, obtains a complete load-displacement curve, and provides a theoretical basis for the quality evaluation and modelling analysis on grouted soil anchors.

Keywords: Load-displacement curve, Ultimate bearing capacity, Grouted soil anchors, Interface shear model, Entire pullout process

1. Introduction

A large number of artificial slopes and underground tunnels have been built with the rapid construction of transport facilities, such as roads and railways. Although numerous engineering measures have been conducted to support the slopes and tunnels, the slope instability, tunnel collapse, serious deformation on the retaining structure of slopes and tunnels, and other problems are obvious. In this case, anchors have been utilized to support the slopes and tunnels. Anchors rationally use the strength and stability of geomaterials to control their deformation, and effectively prevent their collapse or instability. Anchors prevent the instability and serious deformation of slopes and tunnels and effectively reduce the sectional size of retaining structures, such as slope retaining walls and tunnel linings. Thus, anchors are widely used in landslide control, high slope support, and reinforcement on surrounding rocks of tunnels and other projects [1, 2].

For the reinforcement with anchors, the quality of anchors plays a crucial role in the reinforcement stability. For the quality test of anchors, a bearing capacity test is an important link and its fundamental purpose is to determine the load-displacement curve and ultimate bearing capacity of

anchors. For the stability analysis on the combined supporting structure of anchors, the effect of anchors on the retaining structure is generally equivalent to a tension spring and the constitutive relation of the spring is quantitatively described by the load-displacement curve of anchors. To evaluate the quality of anchors and analyze the stability on the combined supporting structure of anchors, the complete load-displacement curve of anchors in the pullout process should be accurately obtained.

Three types of anchors, namely, mechanical, grouted, and friction anchors, are used [3]. Among the anchors, grouted anchors are widely used in engineering practice due to their convenient construction, low cost, and flexible application. This study mainly focuses on grouted anchors in soil. A grouted soil anchor is a composite system composed of an anchoring section (bolt and grout), surrounding soil mass, and the contact surface between them [4]. The shear properties of the interface between the anchoring section and soil mass are important for the study on the pullout characteristics of grouted soil anchors. The analytical solutions for the load-displacement curve of anchors can be obtained by using a shear model of anchor-soil interface [5]. However, existing analytical methods only solve the partial pullout process of grouted soil anchors, obtain the local load-displacement curve, and cannot obtain a complete load-displacement curve.

On this basis, the mathematical model for the entire pullout process of grouted soil anchors was established

*E-mail address: cjj77928@126.com

ISSN: 1791-2377 © 2018 Eastern Macedonia and Thrace Institute of Technology. All rights reserved.

doi:10.25103/jestr.113.05

based on the softening shear model of anchor-soil interface and the load transfer model of anchoring section in this study. The pullout force of anchors was calculated by numerical simulation, and a complete load-displacement curve was obtained, which provide reference for the quality test and modeling analysis on anchors.

2. State of the art

Anchors as practical reinforcements are widely used in engineering constructions because of their reliable technology and good economic benefits [6-8]. However, the theoretical research on anchor system is relatively inadequate because it has a complex stress mechanism that involves many factors. The transmission of pulling force is gradual in the pullout process of anchors. The pulling force of anchors is transferred from the anchor rod to the anchoring section and is spread to the surrounding rock-soil mass through the bonding force between the anchoring section and rock-soil mass [9, 10]. Pullout failure mainly occurs along the interface between the anchoring section and surrounding rock-soil mass [11-12]. Thus, the shear properties of the interface between the anchoring section and rock-soil mass are particularly important for investigating the load-displacement curve and ultimate bearing capacity of anchors.

Chen et al. [13] adopted a tri-linear shear model to completely consider the bonding, softening, and debonding processes of the interface, theoretically analyzed the pullout properties of fully grouted anchors, and verified the results of theoretical analysis by a tension test. The results showed that the theoretical method obtained the ultimate pullout load of anchors with different anchorage lengths and shear stress distribution of the anchoring section in the pullout process, which coincided with the test results. However, no specific calculation method was given for the load-displacement relationship of anchors in the study. On the basis of the tri-linear shear model of the interface, Nemcik et al. [14] conducted a numerical simulation analysis on the pullout process of anchors using FLAC2D and obtained the shear stress distribution of the interface and load-displacement curve of anchors. On the basis of a softening shear model of the interface, Martin et al. [15, 16] obtained the shear stress distribution and load-displacement curve of rock bolts combined with the load transfer differential equation of the anchoring section. The load-displacement relationship of anchors in the pullout process was easily obtained by using the abovementioned analytical methods. However, the abovementioned studies were all based on rock bolts, and few studies were reported on soil bolts. To improve the application of anchorage theories in geotechnical engineering, the shear model of the anchor-soil interface and load-deformation characteristics of anchors in soil should be investigated.

Considering the similarity between the anchor-soil and pile-soil interfaces and mature research on the shear model of pile-soil interface [17, 18], most previous studies on the shear model of anchor-soil interface utilized the relevant conclusions of the shear model of pile-soil interface. To investigate the shear characteristics of the anchor-soil interface, Chen et al. [19] developed a tester that simulated the bonding characteristics of anchor-soil interface under various environmental conditions in batches and proposed a new shear model of anchor-soil interface. On the basis of the shear model of anchor-soil interface, the load-deformation

characteristics of the soil anchor in the pullout process were investigated.

Duan et al. [20] utilized the shear model of anchor-soil interface and the basic method of shear displacement to establish a mechanical differential equation and to deduce the theoretical expressions for the critical load of pullout loosening and the relationship between the pullout load and loosening length of soil anchors. They obtained the load-displacement curve of anchors by using the pullout test data of anchors. However, they assumed that the shear model was a single-drop type and only considered the elastic and debonding stages without considering the softening stage in the transition stage. Their assumption only met the bonding characteristics of anchors in special soil layers and did not represent the bonding characteristics in general soil layers. For general soil anchors, Guo et al. [5] deduced the mechanical differential equation of soil anchors, obtained the internal relations among shear stress distribution type, ultimate pullout load, and failure characteristics, and obtained the analytical solution on the load-displacement curve of anchors based on the shear model of bonding-softening-debonding of anchor-soil interface. Their study expanded the application range of anchors in soil layers. However, their study only considered the elastic, elastic-softening, and elastic-softening-debonding stages in the pullout process of anchors and ignored the pullout process of anchors in the softening-debonding and complete debonding stages. Thus, a complete load-displacement curve was not obtained. On this basis, the entire pullout process of anchors was divided into five stages, namely, elastic, elastic-softening, elastic-softening-debonding, softening-debonding, and debonding stages. The mechanical differential equation of anchors in each stage was deduced based on the tri-linear softening model of anchor-soil interface and the load transfer model of anchoring section. A mathematical model for the entire pullout process of anchors was established combined with boundary conditions in this study. Numerical optimization calculation was conducted in MATLAB, and the complete load-displacement curve of anchors was obtained, which provide a basis for the quality test and modeling analysis on grouted soil anchors.

The rest of this study is organized as follows: Section 3 establishes a mathematical model for the entire pullout process of anchors and calculates the load-displacement curve. Section 4 obtains the pullout load-displacement curve of anchors by using the theoretical analysis method in Section 3 based on a specific project case. The curve is compared with the pullout test curve. Section 5 provides the relevant conclusions.

3. Methodology

3.1 Mechanical Model of Anchors under Pullout Force

Under normal circumstances, the shear strength of the interface between the grout and soil is smaller than that between the grout and bolt. Thus, pullout failures mainly occur along the interface between the grout and soil. For the convenience of calculation, the bolt and grout are regarded as a whole (anchoring section) that is equivalent to a solid rod. The effect of surrounding soil on the anchoring section is regarded as a series of nonlinear bonding springs that acts on the interface. The mechanical model of anchors under pullout force is shown in Fig. 1.

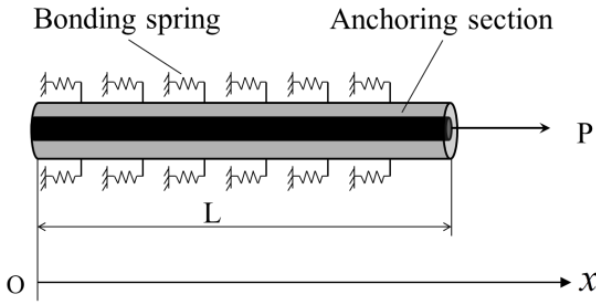


Fig. 1. Mechanical model of the anchors

3.1.1 Softening Shear Model of Anchor-Soil Interface

This study assumes that anchor damages mainly occur at the interface between the anchoring section (including the bolt and grout) and soil, and the anchoring section remains in a linear elastic stage during the pullout process. The shear model of bond springs that act on the anchoring section is quantitatively described by the shear stress-displacement relationship of anchor-soil interface. The shear stress at any point on the anchor-soil interface is composed of bonding force, mechanical interlocking force, and friction. The shear stress-displacement curve of the anchor-soil interface is obtained by fitting the experimental data, which is generally represented by a piecewise linear function, as shown in Fig. 2.

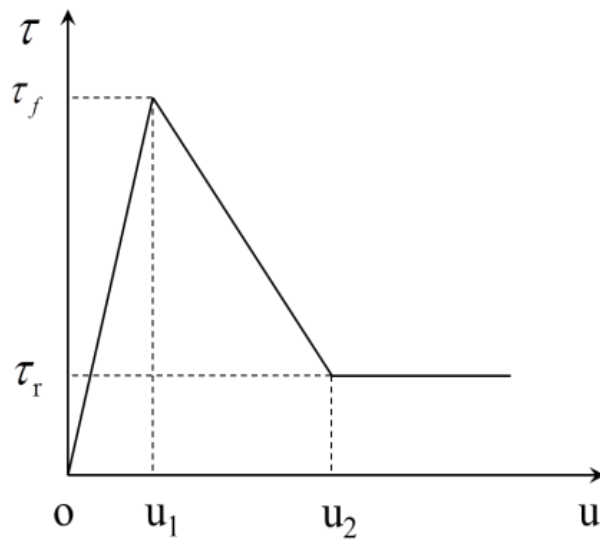


Fig. 2. Softening shear model of the anchor-soil interface

Stage I is the elastic stage, where the deformation between the anchoring section and surrounding soil is coordinated. The shear stress is linearly increased with the shear displacement, and the point on the anchor-soil interface is in a non-destructive bonded state. The shear stress reaches peak shear strength τ_f when the shear displacement increases to u_1 . The surface enters Stage II with the increase of shear displacement, which is called the softening stage. At this stage, uncoordinated deformation occurs between the anchoring section and surrounding soil. The bonding and mechanical interlocking forces gradually fail, and shear stress decreases. The bonding and mechanical interlocking forces completely fail and only friction exists when the shear displacement reaches u_2 . The shear stress

reaches residual strength τ_r . The shear stress maintains its residual strength with the arbitrary development of shear deformation when the shear displacement exceeds u_2 . The interface enters Stage III, which is the debonding stage. The softening shear model of the anchor-soil interface is expressed as

$$\tau(u) = \begin{cases} \frac{\tau_f}{u_1} u & ; \quad 0 \leq u \leq u_1 \quad (a) \\ \frac{\tau_r(u-u_1) + \tau_f(u_2-u)}{u_2-u_1} & ; \quad u_1 \leq u \leq u_2 \quad (b) \\ \tau_r = k\tau_f & ; \quad u \geq u_2 \quad (c) \end{cases} \quad (1)$$

where

$\tau(u)$ is the shear stress of the interface;

τ_f and u_1 are the peak shear strength of the interface and corresponding shear displacement;

τ_r and u_2 are the residual shear strength of the interface and corresponding shear displacement; and

k is the residual coefficient, which is equal to the ratio of residual shear strength to peak shear strength with a value range of $0 \leq k \leq 1$.

3.1.2 Fundamental Differential Equation for the Load Transfer of Anchoring Section

The radius of anchoring section is set as r , and an element with a length of dx is used for stress analysis, as shown in Fig. 3.

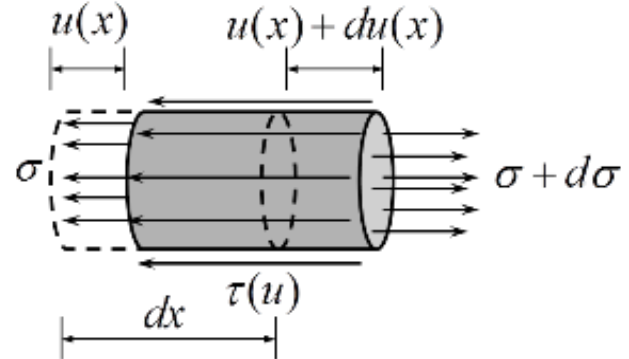


Fig. 3. Mechanical model of the element

The static equilibrium equation for the element is:

$$\pi r^2 \sigma + 2\pi r \tau(u) dx = \pi r^2 (\sigma + d\sigma) \quad (2)$$

This equation can be simplified as:

$$\frac{d\sigma}{dx} = \frac{2\tau(u)}{r} \quad (3)$$

The physical equation for the element is:

$$\frac{du}{dx} = \frac{\sigma}{E} \quad (4)$$

Where

$$E = \frac{E_g A_g + E_b A_b}{A_g + A_b};$$

E and A are the elastic modulus and cross-sectional area of the anchoring section;

E_g and A_g are the elastic modulus and cross-sectional area of the grout; and

E_b and A_b are the elastic modulus and cross-sectional area of the bolt.

The fundamental differential equation for the load transfer of the anchoring section can be obtained by combining Equations (3) and (4), which is expressed as

$$\frac{d^2u}{dx^2} - \frac{2\tau(u)}{rE} = 0 \quad (5)$$

3.2 Analytical Solutions for the Entire Pullout Process of the Anchors

With the increase on the pullout displacement of the anchors, the pullout process of the anchoring section can be divided into five stages, namely, elastic, elastic-softening, elastic-softening-debonding, softening-debonding, and debonding stages. The shear stress distribution at each stage is shown in Fig. 4.

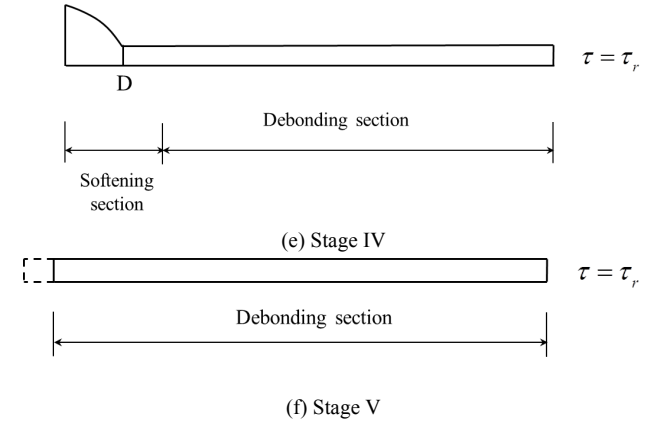
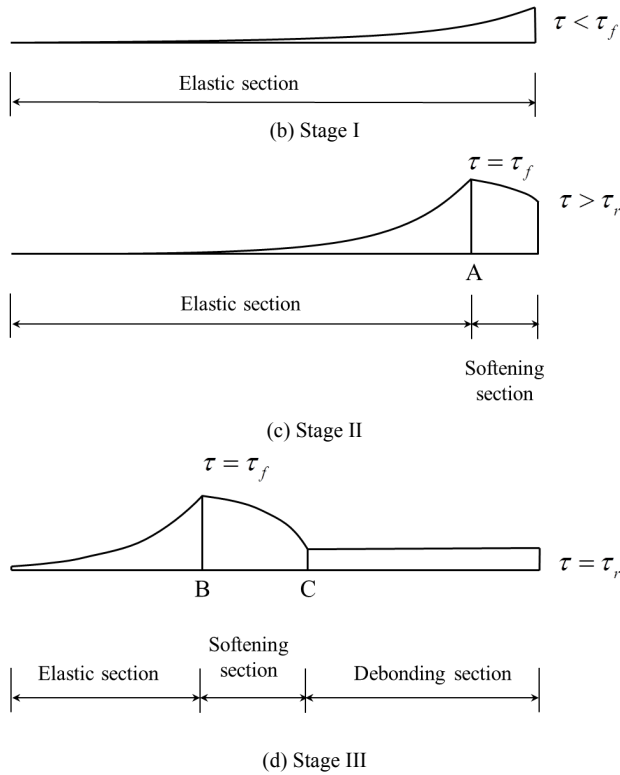
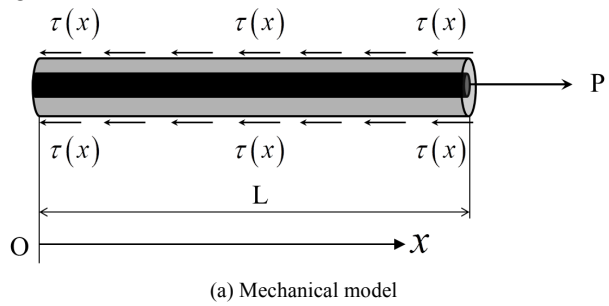


Fig. 4. Evolution of shear stress distribution along the anchor-soil interface in the pullout process

3.2.1 Stage I (Elastic Stage)

At the initial stage of tensioning, the pullout displacement is small and the entire anchor-soil interface is elastic. At this moment, anchor end displacement u_L satisfies $0 \leq u_L \leq u_1$, as shown in Fig. 4(b). The fundamental differential equation for the first stage can be obtained by combining Equation (1a) with Equation (5):

$$\frac{d^2u}{dx^2} - \lambda_1^2 u = 0 \quad ; \quad 0 \leq x \leq L \quad (6)$$

$$\text{where } \lambda_1^2 = \frac{2\tau_f}{ru_1 E}.$$

The general solution to Equation (6) is

$$u(x) = C_1 e^{\lambda_1 x} + C_2 e^{-\lambda_1 x} \quad (7)$$

On the basis of boundary conditions $\sigma_{x=0} = 0$ and $0 \leq u_L \leq u_1$, the solution is obtained as

$$C_1 = C_2 = \frac{u_L}{2 \cosh(\lambda_1 L)} \quad (8)$$

The displacement solution is

$$u(x) = \frac{u_L \cosh(\lambda_1 x)}{\cosh(\lambda_1 L)} \quad (9)$$

The corresponding shear stress and axial force of the anchoring section are expressed as

$$\tau(x) = \frac{\tau_f u_L \cosh(\lambda_1 x)}{u_1 \cosh(\lambda_1 L)} \quad (10)$$

$$\varepsilon(x) = \frac{u_L \lambda_1 \sinh(\lambda_1 x)}{\cosh(\lambda_1 L)} \quad (11)$$

3.2.2 Stage II (Elastic-Softening Stage)

The anchor-soil interface inside and outside is in elastic and softening states when the pullout displacement increases and

displacement u_L satisfies $u_1 < u_L \leq u_2$. The coordinates of boundary point A are $x = a$, as shown in Fig. 4(c). The fundamental differential equations for the elastic and softening stages can be obtained by combining Equations (1a) and (1b) with Equation (5):

$$\begin{cases} \frac{d^2u}{dx^2} + \lambda_1^2 u = 0 & ; \quad 0 \leq x \leq a \\ \frac{d^2u}{dx^2} + \lambda_2^2(1-k)u - \lambda_2^2(u_2 - ku_1) = 0 & ; \quad a \leq x \leq L \end{cases} \quad (12)$$

$$\text{where } \lambda_2^2 = \frac{2\tau_f}{rE(u_2 - u_1)}.$$

The boundary conditions are $\sigma_{x=0} = 0$, $\varepsilon_{x=a^-} = \varepsilon_{x=a^+}$, $u_{x=a^-} = u_{x=a^+} = u_1$, and $u_1 \leq u_L \leq u_2$.

(1) Elastic section ($0 \leq x \leq a$)

The displacement, shear stress, and axial force in the elastic section are similar to that of Equations (9) to (11). Length L and displacement u_L are replaced with a and u_1 . The general solution for the second equation in Equation (12) is

$$u(x) = \frac{u_1 \cosh(\lambda_1 x)}{\cosh(\lambda_1 a)} \quad (13)$$

$$\tau(x) = \frac{\tau_f \cosh(\lambda_1 x)}{\cosh(\lambda_1 a)} \quad (14)$$

$$\varepsilon(x) = \frac{u_1 \lambda_1 \sinh(\lambda_1 x)}{\sinh(\lambda_1 a)} \quad (15)$$

$$u(x) = \frac{(u_L - M) \sin[\lambda_2(x-a)\sqrt{1-k}] + (u_1 - M) \sin[\lambda_2(L-x)\sqrt{1-k}]}{\sin[\lambda_2(L-a)\sqrt{1-k}]} + M \quad (21)$$

$$\tau(x) = \frac{\tau_f \sin[\lambda_2(L-x)\sqrt{1-k}] - \frac{\tau_f(1-k)(u_L - M)}{u_2 - u_1} \sin[\lambda_2(x-a)\sqrt{1-k}]}{\sin[\lambda_2(L-a)\sqrt{1-k}]} \quad (22)$$

$$\varepsilon(x) = \frac{\lambda_2 \sqrt{1-k} \left\{ (u_L - M) \cos[\lambda_2(x-a)\sqrt{1-k}] - (u_1 - M) \cos[\lambda_2(L-x)\sqrt{1-k}] \right\}}{\sin[\lambda_2(L-a)\sqrt{1-k}]} \quad (23)$$

(3) Coordinates of boundary point A

On the basis of boundary condition $\varepsilon_{x=a^-} = \varepsilon_{x=a^+}$, Equation (24) is obtained. The value of a can be obtained by Equation (24), which is a nonlinear equation with one unknown quantity.

(2) Softening section ($a \leq x \leq L$)

The general solution in the softening section is

$$u(x) = C_3 \sin(\lambda_2 x \sqrt{1-k}) + C_4 \cos(\lambda_2 x \sqrt{1-k}) + M \quad (16)$$

where,

$$M = \frac{u_1 - ku_2}{1-k}.$$

The following equations are obtained by inserting the boundary conditions:

$$u_1 = C_3 \sin(\lambda_2 a \sqrt{1-k}) + C_4 \cos(\lambda_2 a \sqrt{1-k}) + M \quad (17)$$

$$u_L = C_3 \sin(\lambda_2 L \sqrt{1-k}) + C_4 \cos(\lambda_2 L \sqrt{1-k}) + M \quad (18)$$

The solution can be obtained by combining Equations (17) and (18):

$$C_3 = \frac{(u_L - M) \cos(\lambda_2 a \sqrt{1-k}) - (u_1 - M) \cos(\lambda_2 L \sqrt{1-k})}{\sin[\lambda_2(L-a)\sqrt{1-k}]} \quad (19)$$

$$C_4 = \frac{-(u_L - M) \sin(\lambda_2 a \sqrt{1-k}) + (u_1 - M) \sin(\lambda_2 L \sqrt{1-k})}{\sin[\lambda_2(L-a)\sqrt{1-k}]} \quad (20)$$

The following equations are obtained by combining the two above equations with Equation (16):

$$\begin{aligned} \lambda_1 u_1 \tanh(\lambda_1 a) &= \frac{\lambda_2 \sqrt{1-k}}{\sin[\lambda_2(L-a)\sqrt{1-k}]} \times \left\{ (u_L - M) \right. \\ &\quad \left. - (u_1 - M) \cos[\lambda_2(L-a)\sqrt{1-k}] \right\} \end{aligned} \quad (24)$$

3.2.3 Stage III (Elastic-Softening-Debonding Stage)

The anchor-soil interface inside and outside is in a stress state in the elastic, softening, and debonding stages, as shown in Fig. 4(d). The boundary points between the elastic

and softening sections and between the softening and debonding sections are set as B ($x = b$) and C ($x = c$), respectively. The fundamental differential equation for the anchoring section at this stage can be obtained by combining Equation (1) with Equation (5):

$$\begin{cases} \frac{d^2u}{dx^2} - \lambda_1^2 u = 0 & ; \quad 0 \leq x \leq b \\ \frac{d^2u}{dx^2} + \lambda_2^2 (1-k)u - \lambda_2^2 (u_2 - ku_3) = 0 & ; \quad b \leq x \leq c \\ \frac{d^2u}{dx^2} - \lambda_3^2 u = 0 & ; \quad c \leq x \leq L \end{cases} \quad (25)$$

$$\text{where } \lambda_3^2 = \frac{2k\tau_f}{rE}.$$

The boundary conditions are $\sigma_{x=0} = 0$, $\varepsilon_{x=b^-} = \varepsilon_{x=b^+}$, $u_{x=b^-} = u_{x=b^+} = u_1$, $\varepsilon_{x=c^-} = \varepsilon_{x=c^+}$, $u_{x=c^-} = u_{x=c^+} = u_2$, and $u_2 < u_L \leq u_3$.

u_3 is the pullout displacement of the anchor end in a critical transition state from the third to fourth stage.

$$u(x) = \frac{(u_2 - M) \sin[\lambda_2(x-b)\sqrt{1-k}] + (u_1 - M) \sin[\lambda_2(c-x)\sqrt{1-k}]}{\sin[\lambda_2(c-b)\sqrt{1-k}]} + M \quad (29)$$

$$\tau(x) = \frac{\tau_f \sin[\lambda_2(c-x)\sqrt{1-k}] + \tau_f k \sin[\lambda_2(x-b)\sqrt{1-k}]}{\sin[\lambda_2(c-b)\sqrt{1-k}]} \quad (30)$$

$$\varepsilon(x) = \frac{\lambda_2 \sqrt{1-k} \{ (u_L - M) \cos[\lambda_2(x-a)\sqrt{1-k}] - (u_1 - M) \cos[\lambda_2(L-x)\sqrt{1-k}] \}}{\sin[\lambda_2(L-a)\sqrt{1-k}]} \quad (31)$$

(3) Debonding section ($c \leq x \leq L$)

The general solution in the debonding section is

$$u(x) = \frac{\lambda_3^2}{2} (x + C_5)^2 + C_6 \quad (32)$$

The following equations can be obtained after placing the boundary conditions in Equation (32):

$$u_2 = \frac{\lambda_3^2}{2} (c + C_5)^2 + C_6 \quad (33)$$

$$u_L = \frac{\lambda_3^2}{2} (L + C_5)^2 + C_6 \quad (34)$$

The following equations can be obtained after combining Equations (33) and (34):

$$C_5 = \frac{u_L - u_2}{(L-c)\lambda_3^2} - \frac{L+c}{2} \quad (35)$$

(1) Elastic section ($0 \leq x \leq b$)

The following equations are obtained by replacing length L and displacement u_L in Equations (9) to (11) with b and u_1 , respectively:

$$u(x) = \frac{u_1 \cosh(\lambda_1 x)}{\cosh(\lambda_1 b)} \quad (26)$$

$$\tau(x) = \frac{\tau_f \cosh(\lambda_1 x)}{\cosh(\lambda_1 b)} \quad (27)$$

$$\varepsilon(x) = \frac{u_1 \lambda_1 \sinh(\lambda_1 x)}{\sinh(\lambda_1 b)} \quad (28)$$

(2) Softening section ($b \leq x \leq c$)

The following equations are obtained by replacing a, L, and u_L in Equations (21) to (23) with b, c, and u_2 , respectively:

$$C_6 = u_L - \frac{\lambda_3^2}{2} \left[\frac{u_L - u_2}{(L-c)\lambda_3^2} + \frac{L-c}{2} \right]^2 \quad (36)$$

$$u(x) = u_L + \frac{\lambda_3^2}{2} \left(x + \frac{u_L - u_2}{(L-c)\lambda_3^2} - \frac{L-c}{2} \right)^2 - \frac{\lambda_3^2}{2} \left[\frac{u_L - u_2}{(L-c)\lambda_3^2} + \frac{L-c}{2} \right]^2 \quad (37)$$

The corresponding shear stress and axial force are expressed as:

$$\tau(x) = \tau_r = k\tau_f \quad (38)$$

$$\varepsilon(x) = \lambda_3^2 x + \frac{u_L - u_2}{(L-c)} - \frac{L-c}{2} \lambda_3^2 \quad (39)$$

(4) Coordinates of boundary points b and c, and u_3

For different u_L values, the corresponding coordinates of boundary points b and c can be obtained with the continuity

conditions of two points. Equation (40) can be obtained with $\varepsilon_{x=b^-} = \varepsilon_{x=b^+}$ and $\varepsilon_{x=c^-} = \varepsilon_{x=c^+}$. The values of b and c can be obtained by Equation (40), which is a nonlinear equation with two unknown quantities. The anchor is in a critical transition state from the third to fourth stage when $b = 0$.

$$\left\{ \begin{array}{l} \lambda_1 u_1 \tanh(\lambda_1 b) = \frac{\lambda_2 \sqrt{1-k} \left\{ (u_2 - M) - (u_1 - M) \cos[\lambda_2(c-b)\sqrt{1-k}] \right\}}{\sin[\lambda_2(c-b)\sqrt{1-k}]} \\ \frac{\lambda_2 \sqrt{1-k} \left\{ (u_2 - M) \cos[\lambda_2(c-b)\sqrt{1-k}] - (u_1 - M) \right\}}{\sin[\lambda_2(c-b)\sqrt{1-k}]} = \frac{u_L - u_2}{(L-c)} - \frac{L-c}{2} \lambda_3^2 \end{array} \right. \quad (40)$$

$$\left\{ \begin{array}{l} \frac{\lambda_2 \sqrt{1-k} [(u_2 - M) - (u_1 - M) \cos(\lambda_2 c \sqrt{1-k})]}{\sin(\lambda_2 c \sqrt{1-k})} = 0 \\ \frac{u_L - u_2}{(L-c)} - \frac{L-c}{2} \lambda_3^2 = \frac{\lambda_2 \sqrt{1-k} [(u_2 - M) \cos(\lambda_2 c \sqrt{1-k}) - (u_1 - M)]}{\sin(\lambda_2 c \sqrt{1-k})} \end{array} \right. \quad (41)$$

3.2.4 Stage IV (Softening-Debonding Stage)

The anchor-soil interface is in a stress state in the softening and debonding stages, which are distributed inside and outside of the anchoring section, as shown in Fig. 4(e). The boundary point between the two sections is set as D ($x = d$). Fundamental differential equations of the softening and debonding sections can be obtained by combining Equations (1b) and (1c) with Equation (5):

$$\left\{ \begin{array}{ll} \frac{d^2 u}{dx^2} + \lambda_2^2 (1-k) u - \lambda_2^2 (u - k u_1) = 0 & ; \quad 0 \leq x \leq d \\ \frac{d^2 u}{dx^2} - \lambda_3^2 = 0 & ; \quad d \leq x \leq L \end{array} \right. \quad (42)$$

The boundary conditions are $\sigma_{x=0} = 0$, $\varepsilon_{x=d^-} = \varepsilon_{x=d^+}$, $u_{x=d^-} = u_{x=d^+} = u_2$, and $u_3 < u_L \leq u_4$.

u_4 is the pullout displacement of the anchor end when the anchor is in a critical transition state from the fourth to fifth stage.

(1) Softening section ($0 \leq x \leq d$)

Based on Equations (21) to (23), the solutions are

$$u(x) = -\frac{k(u_2 - u_1)}{1-k} \frac{\cos(\lambda_2 x \sqrt{1-k})}{\cos(\lambda_2 d \sqrt{1-k})} + \frac{u_2 - k u_1}{1-k} \quad (43)$$

$$\tau(x) = \frac{k \tau_f \cos(\lambda_2 x \sqrt{1-k})}{\cos(\lambda_2 d \sqrt{1-k})} \quad (44)$$

$$\varepsilon(x) = \frac{k \lambda_2 (u_2 - u_1)}{\sqrt{1-k}} \frac{\sin(\lambda_2 x \sqrt{1-k})}{\cos(\lambda_2 d \sqrt{1-k})} \quad (45)$$

(2) Debonding section ($d \leq x \leq L$)

Equation (41) is obtained by combining $b = 0$ with Equation (40). The values of end displacement u_3 and boundary point c in the critical state can be obtained by Equation (41).

Based on Equations (37) to (39), the solutions are

$$u(x) = u_L + \frac{\lambda_3^2}{2} \left(x + \frac{u_L - u_2}{(L-d)\lambda_3^2} - \frac{L+d}{2} \right)^2 - \frac{\lambda_3^2}{2} \left[\frac{u_L - u_2}{(L-d)\lambda_3^2} + \frac{L-d}{2} \right]^2 \quad (46)$$

$$\tau(x) = \tau_r = k \tau_f \quad (47)$$

$$\varepsilon(x) = \lambda_3^2 x + \frac{u_L - u_2}{L-d} - \frac{L+d}{2} \lambda_3^2 \quad (48)$$

(3) Determination of d and u_4

On the basis of the continuity conditions of D, the following equation can be obtained:

$$\frac{k \lambda_2 (u_2 - u_1)}{\sqrt{1-k}} \tan(\lambda_2 d \sqrt{1-k}) = \frac{u_L - u_2}{L-d} - \frac{L-d}{2} \lambda_3^2 \quad (49)$$

The value of d can be obtained by Equation (49), which is a nonlinear equation with one unknown quantity.

The anchor is in a critical transition state from the fourth to fifth stage when $d = 0$. On the basis of Equation (49), the displacement of the anchors in the critical state is

$$u_4 = \frac{\lambda_3^2}{2} L^2 + u_2 \quad (50)$$

3.2.5 Stage IV (Softening-Debonding Stage)

The anchor is gradually removed when the pullout displacement of the anchor end increases from u_4 , as shown in Fig. 4(f). The contact length between the anchoring section and surrounding soil decreases. The pullout load decreases with the increase of pullout displacement. The shear stress of the interface is the residual shear stress

$$\tau(x) = \tau_r = k\tau_f \quad (51)$$

3.3 Computational Simulation of Load-Displacement Curve of Anchors

On the basis of the mathematical model for the entire pullout process of the anchors established in 3.2, the computational simulation can be conducted to obtain the complete load-displacement curve and determine the ultimate bearing capacity of the anchors.

(1) In Stage I, the strain of the anchor end can be obtained with Equation (11)

$$\varepsilon(L) = u_L \lambda_1 \tanh(\lambda_1 L) \quad (52)$$

Therefore, the load-displacement relationship of the anchor end is:

$$P = EA \lambda_1 \tanh(\lambda_1 L) u_L ; \quad 0 \leq u_L \leq u_1 \quad (53)$$

(2) In Stage II, the strain of the anchor end can be obtained with Equation (23)

$$\varepsilon(x) = \frac{\lambda_2 \sqrt{1-k} \left\{ (u_L - M) \cos \left[\lambda_2 (L-a) \sqrt{1-k} \right] + (u_1 - M) \right\}}{\sin \left[\lambda_2 (L-a) \sqrt{1-k} \right]} \quad (54)$$

Therefore, the load-displacement relationship of the anchor end is:

$$P = \frac{-\lambda_2 EA \sqrt{1-k}}{\sin \left[\lambda_2 (L-a) \sqrt{1-k} \right]} \left\{ (u_1 - M) - (u_L - M) \cos \left[\lambda_2 (L-a) \sqrt{1-k} \right] \right\} ; \quad u_1 \leq u_L \leq u_2 \quad (55)$$

(3) In Stage III, the strain of the anchor end can be obtained with Equation (39)

$$\varepsilon(L) = \lambda_3^2 L + \frac{u_L - u_2}{L - c} - \frac{L + c}{2} \lambda_3^2 \quad (56)$$

Therefore, the load-displacement relationship of the anchor end is:

$$P = EA \left(\lambda_3^2 L + \frac{u_L - u_2}{L - c} - \frac{L + c}{2} \lambda_3^2 \right) ; \quad u_2 \leq u_L \leq u_3 \quad (57)$$

(4) In Stage IV, the strain of the anchor end can be obtained with Equation (48):

$$\varepsilon(L) = \lambda_3^2 L + \frac{u_L - u_2}{L - d} - \frac{L + d}{2} \lambda_3^2 \quad (58)$$

Therefore, the load-displacement relationship of the anchor end is:

$$P = EA \left(\lambda_3^2 L + \frac{u_L - u_2}{L - d} - \frac{L + d}{2} \lambda_3^2 \right) ; \quad u_3 \leq u_L \leq u_4 \quad (59)$$

(5) In Stage V, the strain of the anchor end can be obtained with Equation (48). The pullout load is balanced by the residual shear strength on the anchoring section, and its pullout load-displacement relationship is:

$$P = 2k\pi r \tau_f (L - u_4 - u) ; \quad u_4 \leq u \leq L - u_4 \quad (60)$$

In the above equations, the values of a, b, c, and d are determined by nonlinear equations or equation sets (24), (40), and (49). The fmincon function provided by MATLAB can be used for solution [21]. The function only requires an F-function module and an initial value, and its minimum value can be searched without derivation. The search is quick provided that a suitable initial value is given.

4 Result Analysis and Discussion

To explain the specific application of the proposed method in engineering practice, a field pullout test was conducted in a deep foundation pit of a high-rise building in Chongqing. The theoretical analysis results and test results in Part 3 were analyzed to verify the accuracy of the proposed method. The maximum excavation depth of the foundation pit engineering was 22.5 m, and the supporting structure with anchor pile wall was adopted. The test anchor was buried in the piles. The inclination of the anchor was 15°, the drilling diameter was 150 mm and the design length L was 16 m, in which the lengths of the free section and anchorage were 4 and 12 m. The anchoring section was located in a silty clay layer. The density of silty clay layer was $\rho = 1930 \text{ kg/m}^3$, the cohesion was $c = 29.1 \text{ KPa}$, the internal friction angle was $\varphi = 18.9^\circ$, the elastic modulus was 22.5 MPa, and the Poisson's ratio was 0.3.

The anchor adopted a Φ32 screw-thread steel with an elastic modulus of $E_s = 200 \text{ GPa}$. The grouting adopted a cement mortar in which the water-cement ratio was 0.5, the grouting intensity was M30, and the elastic modulus was $E_m = 30 \text{ GPa}$. The anchor was tensioned under various degrees of pullout force after the grout reached the design intensity. The position of measuring points on the anchoring section is shown in Fig. 5.

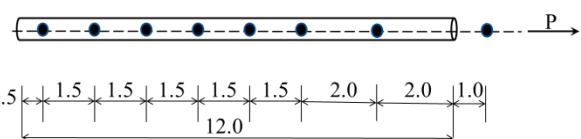


Fig. 5. Position of measuring points on the anchoring section

4.1 Shear stress-displacement curve of the anchor-soil interface

During the tensioning process of the anchor, a tri-linear shear stress-displacement curve of the anchor-soil interface can be fitted by collecting data of measuring points on the anchoring section, as shown in Fig. 6. The corresponding model parameters are $\tau_f = 75.3 \text{ KPa}$, $\tau_r = 33.9 \text{ KPa}$, $u_1 = 3.5 \text{ mm}$, and $u_2 = 5.8 \text{ mm}$.

4.2 Load-Displacement Curve

The experimental curves of load-displacement can be fitted by analyzing the collected data in the field, as shown by the solid blue line in Fig. 7. In addition, the load-displacement curve of the entire pullout process can be obtained by using the model parameters of the anchor-soil interface based on the proposed method in Section 3.3, as shown by the dotted red line in Fig. 7. By comparison, the obtained load-displacement curve in this study is highly consistent with the field experimental data. This finding indicates that the proposed method accurately simulates the pullout process of grouted soil anchors and determines the ultimate bearing capacity of anchors. In addition, the proposed method predicts the descending and residual sections of load-displacement to obtain the complete load-displacement curve.

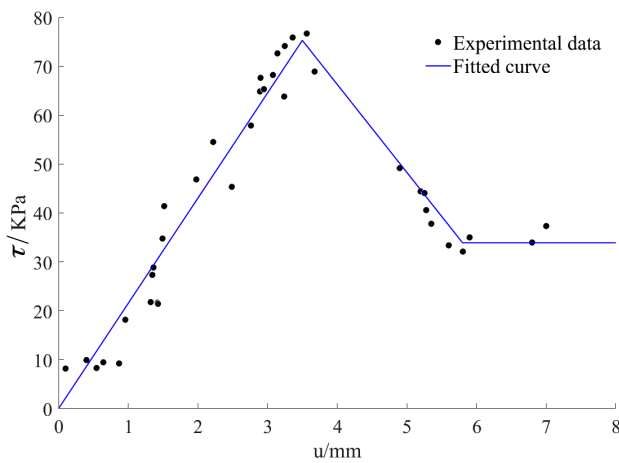


Fig. 6. Shear stress-displacement curve of the anchor-soil interface

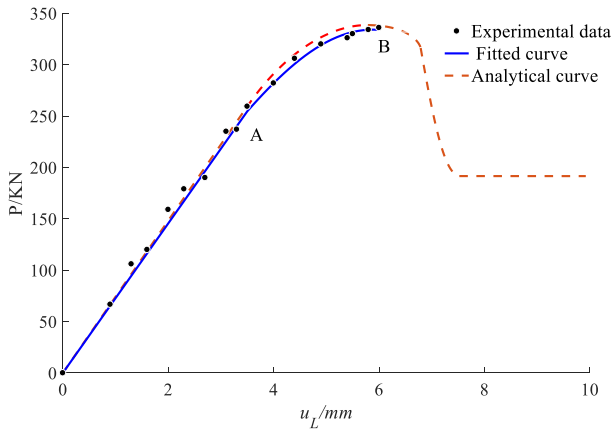
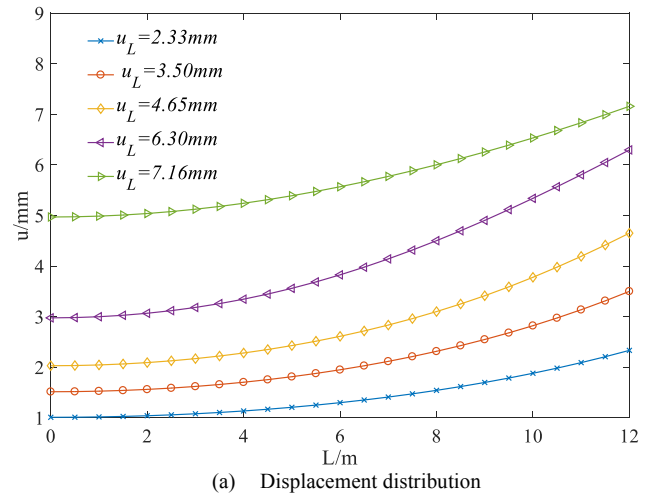


Fig. 7. Load-displacement curve of the anchors

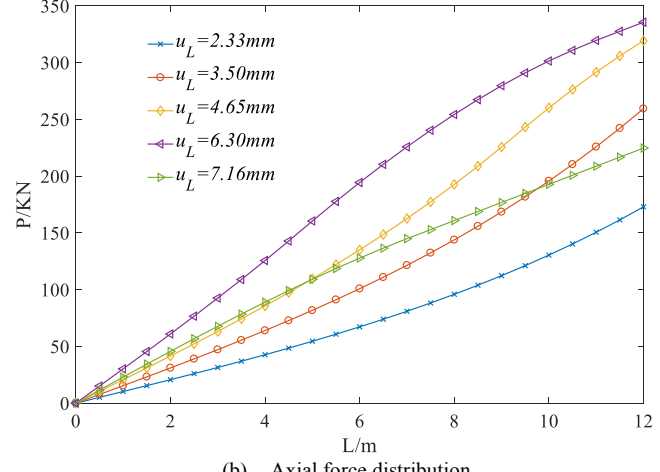
4.2 Distribution of Shear Displacement, Axial Force, and Shear Stress

On the basis of the model parameters of the anchor-soil interface, the displacement, axial force, and shear stress distributions of the anchoring section for different displacements ($u_L = 2.33, 3.50, 4.65, 6.30$, and 7.16 mm) can also be obtained by using the method in 3.2, as shown in Fig. 8. The values of shear displacement and axial force reach the maximum at the end of anchoring section ($x = 12 \text{ m}$) and gradually decrease toward the inside of the anchoring section. The shear stress is irregularly distributed in the anchoring section. The entire anchor-soil interface is

elastic, and the value of shear stress reaches the maximum at the end of anchoring section ($x = 12 \text{ m}$) and gradually decreases toward the inside of the anchoring section when the pullout displacement is small ($u_L = 2.33 \text{ mm}$). The maximum shear stress reaches the peak shear strength when u_L is equal to u_1 ($u_L = 3.50 \text{ mm}$). The anchor-soil interface is in the elastic-softening stage and the shear stress reaches the peak shear strength at the intersection between the elastic and softening sections when u_L increases ($u_L = 4.65 \text{ mm}$). The position of maximum shear stress moves toward the inside of the end of anchoring section when u_L increases.



(a) Displacement distribution



(b) Axial force distribution

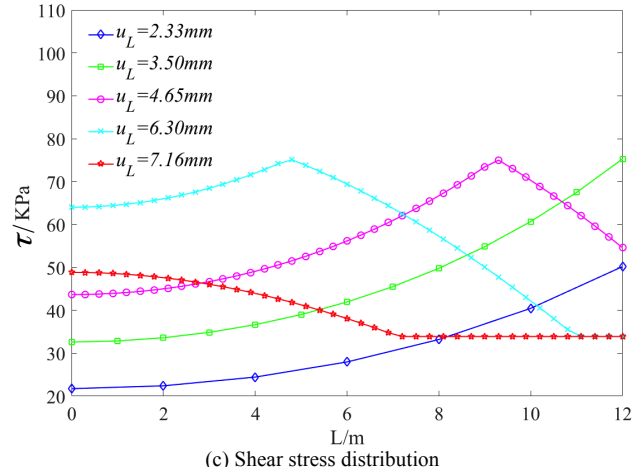


Fig. 8. Displacement, axial force, and shear stress distributions of the anchoring section

4.2 Parameter Analysis

The mechanical properties of soil and the design and construction technologies of anchors affect the pullout properties of anchors. The effect of anchorage length L, anchorage diameter D, elastic modulus of anchoring section E, and residual coefficient k on the load-displacement curve shown in Fig. 9 is analyzed. The influence of different anchorage parameters on load-displacement curves is shown in Fig. 9.

The ultimate pullout load linearly increases and the corresponding displacement gradually increases with the increase of anchorage length. The elastic section slope of the curve and the ultimate pullout load gradually increase when anchorage diameter D increases. The elastic section of the load-displacement curve does not change with the residual coefficient. The ultimate pullout load slightly increases and

the corresponding displacement gradually decreases when residual coefficient k increases. The residual pullout load increases with the increase of length L, diameter D, and residual coefficient k, and does not change with elastic modulus E when the entire anchoring section is in the debonding state. This condition is because the pullout load in the debonding stage mainly depends on the friction on the anchoring section, which is determined by three factors, namely, anchorage diameter, anchorage length, and residual shear strength.

The increase of length L, diameter D, elastic modulus E, and residual shear coefficient k enhance the ultimate pullout load of the anchors to some extent. However, the residual pullout load only increases with the increase of anchorage length L, diameter D, and residual coefficient k, and does not change with elastic modulus E.

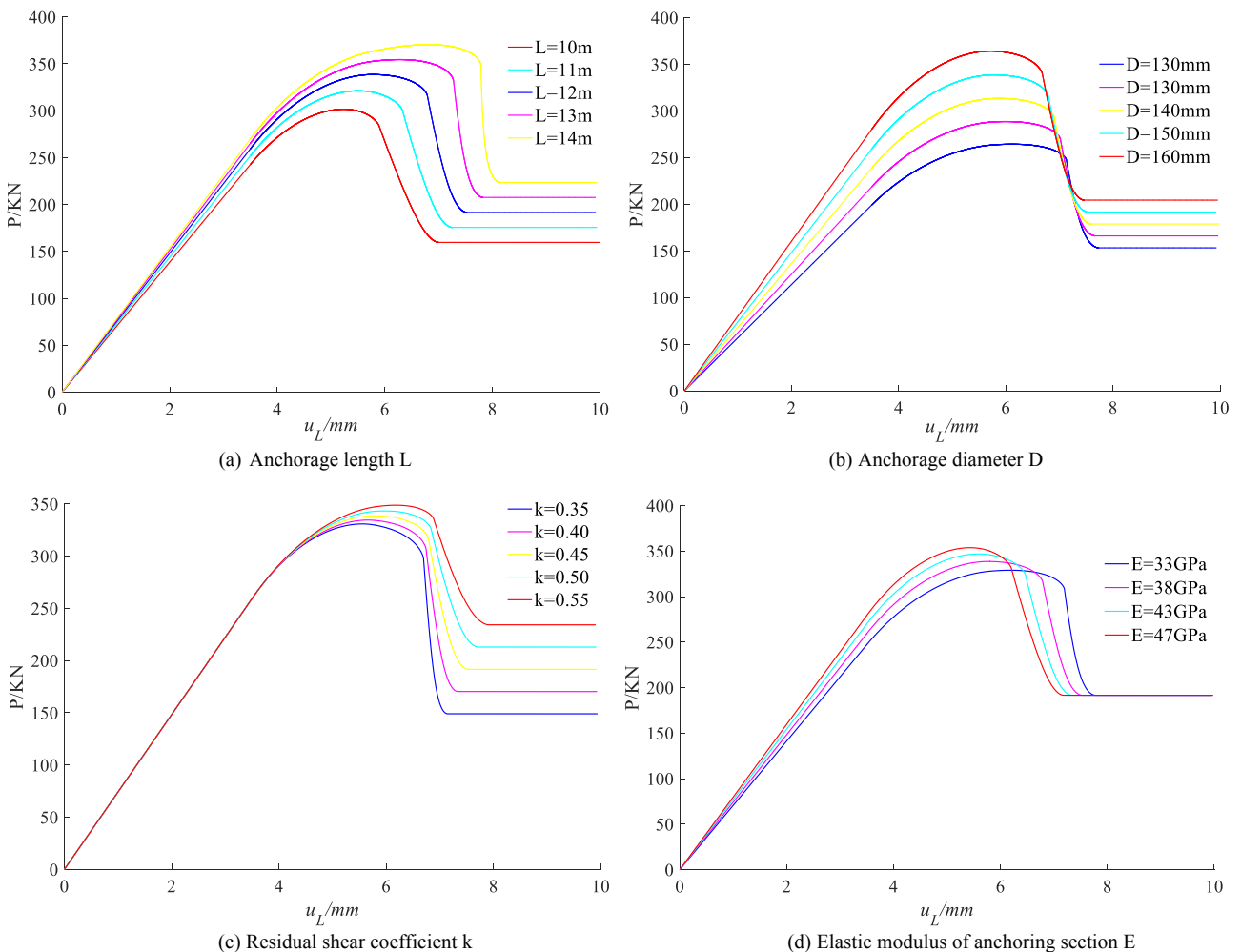


Fig.9. Effects of different parameters on load-displacement curve

5 Conclusions

A mathematical model for the entire pullout process of grouted soil anchors was established to obtain a complete load-displacement curve. The pullout force of anchors was calculated by numerical simulation based on the softening shear model of the anchor-soil interface and load transfer model of the anchoring section. The following major conclusions are summarized as follows:

(1) The entire pullout process of the anchor bolt is accurately simulated in this study. The complete load-displacement curve is obtained with the proposed method, and the theoretical curve is consistent with the field pullout curve.

(2) In the pullout process, the shear stress on the anchoring section is irregularly and non-uniformly distributed with a single peak. The peak point moves to the inner end from the anchor head when the pullout load increases. However, the shear stress on the anchoring section is evenly distributed in the engineering design of anchors.

This assumption is inconsistent with the actual situation. Therefore, modifications should be conducted in the design of anchors.

(3) The changes in anchorage length L, diameter D, residual coefficient k, elastic modulus of anchoring section E, and other parameters influence the load-displacement curve of anchors. The ultimate bearing capacity of anchors increases when L, D, k, and E increase. In the debonding state, the residual pullout load only increases with the increase of anchorage length L, diameter D, and residual coefficient k, and does not change with elastic modulus E.

In summary, a mathematical model for the entire pullout process of grouted soil anchors was established and MATLAB was used for numerical optimization calculation to facilitate programming realization. The proposed method simulates the pullout process of anchors and obtains the complete load-displacement curve, which provides a basis for the quality test and modeling analysis of anchors. However, the theoretical analysis method of the present

study is based on the softening model of anchor-soil interface that is significantly influenced by the surrounding soil of anchors. The model parameters of the anchor-soil interface are different in different soil conditions. Therefore, the application scope of the proposed method should be expanded in future research by introducing the soil parameters in the anchor-soil interface, which will significantly facilitate the understanding on the anchorage mechanism of grouted soil anchors.

Acknowledgements

The authors are grateful for the support provided by the Major Program of the National Natural Science Foundation of China (No. 51638002).

This is an Open Access article distributed under the terms of the Creative Commons Attribution Licence



References

1. Ranjbarnia, M., Fahimifar, A., Oreste, P., "Practical method for the design of pretensioned fully grouted rockbolts in tunnels". *International Journal of Geomechanics*, 16(1), 2016, pp.04015012.
2. Rasekh, H., Mirzaghorbanali, A., Nemcik, J., et al., "A New Equation for the Shear Strength of Cable Bolts Incorporating the Energy Balance Theory". *Geotechnical & Geological Engineering*, 35(4), 2017, pp. 1529-1548..
3. Ren, F., Yang, Z., Chen, J., et al., "An analytical analysis of the full-range behaviour of grouted rockbolts based on a tri-linear bond-slip model". *Construction and Building Materials*, 24(3), 2010, pp. 361-370.
4. Khan, A. J., Mostofa, G., Jadid, R., "Pullout resistance of concrete anchor block embedded in cohesionless soil". *Geomechanics and Engineering*, 12(4), 2017, pp. 675-688.
5. Guo, R., Chen, W., Duan, J., et al., "Pullout mechanical analysis of soil anchor based on softening behavior of interface". *Journal of Central South University(Science and technology)*, 43(10), 2012, pp. 4003-4009.
6. Ranjbarnia, M., Oreste, P., Fahimifar, A., et al., "Analytical-numerical solution for stress distribution around tunnel reinforced by radial fully grouted rockbolts". *International Journal for Numerical and Analytical Methods in Geomechanics*, 40(13), 2016, pp. 1844-1862.
7. Ranjbarnia, M., Fahimifar, A., Oreste, P., "New analytical approaches for evaluating the performance of systematic pretensioned fully grouted rockbolts in tunnel stabilization". *Archives of Mining Sciences*, 61(4), 2016, pp. 823-852.
8. Teymen, A., Kılıç, A., "Effect of grout strength on the stress distribution (tensile) of fully-grouted rockbolts". *Tunnelling and Underground Space Technology*, 77, 2018, pp. 280-287.
9. Ghadimi, M., Sharir, K., Jalalifar, H., "A new analytical solution for calculation the displacement and shear stress of fully grouted rock bolts and numerical verifications". *International Journal of Mining Science and Technology*, 26(6), 2016, pp. 1073-1079.
10. Akisanya, A. R., Ivanović, A., "Debonding along the fixed anchor length of a ground anchorage". *Engineering Structures*, 74, 2014, pp.23-31.
11. Thenevin, I., Blanco-Martín, L., Hadj-Hassen, F., et al., "Laboratory pull-out tests on fully grouted rock bolts and cable bolts: Results and lessons learned". *Journal of Rock Mechanics and Geotechnical Engineering*, 9(5), 2017, pp. 843-855.
12. Saydam, S., Hagan, P. C., Chen, J., "A new laboratory short encapsulation pull test for investigating load transfer behavior of fully grouted cable bolts". *Geotechnical Testing Journal*, 41(3), 2018, doi: 10.1520/GTJ20170139.
13. Chen, J., Saydam, S., Hagan, P. C., "An analytical model of the load transfer behavior of fully grouted cable bolts". *Construction and Building Materials*, 101, 2015, pp. 1006-1015.
14. Nemcik, J., Ma, S., Aziz, N., et al., "Numerical modelling of failure propagation in fully grouted rock bolts subjected to tensile load". *International Journal of Rock Mechanics and Mining Sciences*, 71, 2014, pp. 293-300.
15. Martin, L. B., Tijani, M., Hadj-Hassen, F., "A new analytical solution to the mechanical behaviour of fully grouted rockbolts subjected to pull-out tests". *Construction and Building Materials*, 25(2), 2011, pp. 749-755.
16. Martin, L. B., Tijani, M., Hadj-Hassen, F., et al., "Assessment of the bolt-grout interface behaviour of fully grouted rockbolts from laboratory experiments under axial loads". *International Journal of Rock Mechanics and Mining Sciences*, 63, 2013, pp. 50-61.
17. Aljorany, A. N., Al-Jumaily, F. A., "A computational procedure to predict the load-settlement behavior of axially loaded piles in sandy soils". *Japanese Geotechnical Society Special Publication*, 2(37), 2016, pp. 1343-1347.
18. Boonyatee, T., Lai, Q. V., "A non-linear load transfer method for determining the settlement of piles under vertical loading". *International Journal of Geotechnical Engineering*, 2017, pp. 1-12.
19. Chen, C., Liang, G., Tang, Y., et al., "Anchoring solid-soil interface behavior using a novel laboratory testing technique". *Chinese Journal of Geotechnical Engineering*, (06), 2015, pp. 1115-1122.
20. Duan, J., Yan, Z., Guo, R., et al., "Failure analysis of soil anchors induced by loose interface under pullout load". *Chinese Journal of Geotechnical Engineering*, 34(05), 2012, pp. 936-941.
21. Xue, D. Y., Chen, Y. Q., "Advanced applied mathematical problem solutions with MATLAB". Beijing: Tsinghua University Press, china, 2013.